# Cavitation and Sand Slurry Erosion Resistances of WC-10Co-4Cr Coatings

Qun Wang, Zhaoxi Tang & Limei Cha

**Journal of Materials Engineering and Performance**

ISSN 1059-9495

J. of Materi Eng and Perform
DOI 10.1007/s11665-015-1496-z

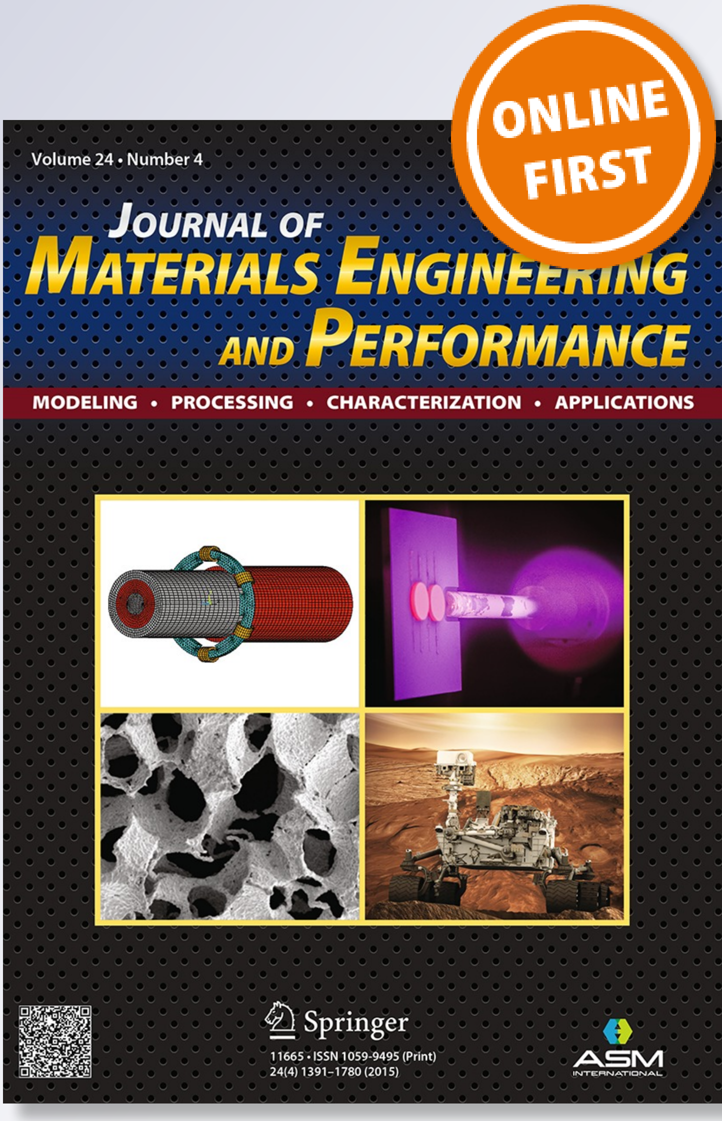

JMEPEG
DOI: 10.1007/s11665-015-1496-z

©ASM International
1059-9495/$19.00

# Cavitation and Sand Slurry Erosion Resistances of WC-10Co-4Cr Coatings

*Qun Wang, Zhaoxi Tang, and Limei Cha*

(Submitted November 5, 2014; in revised form March 19, 2015)

**Two WC-10Co-4Cr coatings were deposited by high-velocity oxygen fuel (HVOF) and high-velocity air fuel (HVAF) spray processes, respectively, and their basic mechanical properties, cavitation and sand slurry erosion resistances were investigated. The results show that the HVAF-sprayed WC-10Co-4Cr coating exhibited a lower degree of decarburization and better properties in terms of hardness, fracture toughness, porosity, cavitation and sand slurry erosion resistances than those of the HVOF-sprayed WC-10Co-4Cr coatings, respectively. Therefore, HVAF-sprayed WC-10Co-4Cr coatings may be better employed for the protection of hydro-turbine component surfaces against cavitation and sand slurry erosion.**

**Keywords** cavitation, HVAF, HVOF, sand slurry erosion, WC-10Co-4Cr

## 1. Introduction

Hydro-turbine components such as guide vanes, runner blades, pivot rings, pump and compressor parts are known to be affected by cavitation and/or sand slurry erosion (Ref 1). During operation, these components are often exposed to a fast-flowing and vibrating liquid under fluctuating pressure. The pressure fluctuation results in the generation and collapse of cavitation bubbles, exerting stress pulses on the nearby solid surface and resulting in its cavitation erosion (Ref 2). In addition, the sand slurry erosion of the hydro-turbine components can hardly be avoided during their service, especially when the large content of hard particles such as $SiO_2$, $Al_2O_3$, $Fe_2O_3$, MgO, CaO, and their compounds are present in the silt. Thus, most of the failures of hydro-turbine components are induced by the combined attack of cavitation and silt-assisted erosion (Ref 1, 3).

In recent years, HVOF-sprayed WC-based coatings have been successfully applied on metal alloy hydro-turbine components to combat cavitation and sand slurry erosion (Ref 4). However, the WC phase in the coatings partially decomposes into $W_2C$ or even W when the traditional HVOF thermal spray technologies are used. It embrittles the coatings and eventually deteriorates their performance (Ref 5, 6). Recently, a high-velocity air fuel (HVAF) system, which operates at a much lower combustion temperature using gas or liquid fuel and compressed air (not oxygen) for combustion, has been investigated (Ref 6–8). It has been found that the deposition of the WC-based coatings by the HVAF spraying process can reduce the production cost due to the use of air instead of pure oxygen, while greatly decreasing the degree of decarburization of WC (Ref 6, 9) or $Cr_3C_2$ (Ref 10) as a result of a much lower flame temperature. Jacobs et al. (Ref 6) have found that WC-based coating deposited by the HVAF spraying method exhibited higher hardness and sliding wear resistance compared to the one applied by the HVOF process. Wang et al. (Ref 11) have also found that the HVAF-sprayed WC-10Co-4Cr coating exhibited higher sliding and abrasive wear resistances as well as higher corrosion resistances than counterpart coatings deposited by gas-fuelled and liquid-fuelled HVOF spray systems.

Generally, fine WC-10Co-4Cr powder (5 to 30 μm) is suitable for the HVAF spray process (AK 07) as a result of its lower flame temperature. While as for the HVOF spray process (DJ2700), the situation is reversed, the fine WC-10Co-4Cr powder usually results in spitting during the spraying process because of the super fusion of the fine powder in the higher temperature flame. Therefore, the coarse powder is much more suitable for the DJ2700 HVOF spray gun (Ref 12).

The WC-10Co-4Cr powder (Amdry 5843, Sulzer-Metco) has been deposited on hydro-turbine components by using the DJ2700 HVOF spraying system to resist cavitation and sand erosion in China for several years. This coating exhibited good sand slurry erosion resistance, but its cavitation resistance was not satisfactory.

In this study, one WC-10Co-4Cr coating was deposited by the HVAF spray process with fine powder. For comparison, a WC-10Co-4Cr coating was prepared by the HVOF spray process with a widely used coarse powder (Amdry 5843). In order to explore whether the HVAF-sprayed WC-10Co-4Cr coating can replace the HVOF one to resist cavitation and sand slurry erosion, the phase compositions, mechanical properties, cavitation and sand slurry erosion resistances of the two WC-10Co-4Cr coatings were investigated.

## 2. Experimental Procedures

### 2.1 Coating Preparation

Two kinds of WC-10Co-4Cr powders were sprayed on low carbon steel substrates by Kermetico's AK 07 HVAF spray system operating with propane and compressed air and Sulzer's DJ2700 HVOF spray system operating with propane, pure oxygen, and air. The powder information and spraying

**Qun Wang, Zhaoxi Tang,** and **Limei Cha,** College of Materials Science and Engineering, Hunan University, Changsha, Hunan 410082, P.R. China. Contact e-mail: wangqun72@163.com.



Published online: 08 April 2015

parameters, listed in Table 1, were suggested by the powder and spray equipment vendors.

Typical characteristics of the two WC-10Co-4Cr powders are presented in Fig. 1.

The WC-10Co-4Cr powder (Amdry 5843) exhibiting irregular-shaped particles (Fig. 1a) were produced by the sintered and crushed process, while the particles of another WC-10Co-4Cr powder (T62M150) were of nearly spherical shape (Fig. 1b), which were produced by the agglomerated and sintered process.

Prior to the spraying process, low carbon steel substrates were degreased and grit blasted with 60-mesh $Al_2O_3$. The thickness of WC-10Co-4Cr coatings deposited on these substrates was approximately 0.3 mm. During spraying, the spraying angle was 90° and the temperatures of the substrates were kept below 150 °C using compressed air cooling.

### 2.2 Characterization

X-ray diffraction (XRD) analysis of the powders and coatings was performed with a Rigaku D/max-2550 diffraction meter using Cu-Ka radiation. The JSM 6700 and FEI-Quanta200 scanning electron microscope was used to examine the morphologies of the powders and coatings. The porosity measurements were performed on the coatings using the image analysis method. The presented porosity was the average values of the data from ten measurements. Hardness measurements were performed on the cross sections of the coatings under the loads of 2.94 and 49 N, respectively, and the hardness reported was the average value of ten measurements. The coating fracture toughness value was calculated using the length of the indentations and cracks according to the Evans and Wilshaw equation (Ref 13). The surface roughness of the sample was measured by Mitutoyo surface roughness tester (SJ 210), and the presented roughness was the average value of five measurements.

### 2.3 Cavitation Erosion

Cavitation erosion tests were performed in a vibratory cavitation apparatus, the specimens (ϕ16 mm) with a screw were attached to the free end of the horn. By controlling the output power of the ultrasonic generator, the system was set in a resonant condition with a frequency of $19 \pm 1$ kHz and a double amplitude of $36 \pm 3$ µm. Pure water was used as the test liquid in a 1000-mL beaker. The beaker was surrounded by cooling water, and the pure water temperature was maintained at 25-30 °C. The tip of the specimen was immersed into the water 3-mm deep. A balance with a sensitivity of 0.1 mg was used to determine the mass losses. The sample was weighed every 60 min and 12 measurements were made. For comparison, the austenitic stainless steel AISI 316 samples were tested under the same experimental conditions.

**Table 1 Powder and spraying equipment parameters for the two WC-10Co-4Cr coatings**

| | DJ coating | AK coating |
|---|---|---|
| Powder code | Amdry 5843(Sulzer-Metco) | T62M150(Achteck) |
| Powder size distribution, µm | 15-53 | 5-30 |
| Powder apparent density, g/cm$^3$ | 5.88 | 5.75 |
| Powder product process | Sintered and crushed | Agglomerated and sintered |
| Spray gun | DJ2700 (HVOF) | AK 07(HVAF) |
| Combustion mixture | Propane: 68 L/min | Propane pressure: 0.50 MPa |
| | Oxygen: 240 L/min, Air: 376 L/min | Air pressure: 0.60 MPa |
| Feed rate, g/min | 45 | 80 |
| Spray distance, mm | 200 | 150 |
| Carrier gas flow, L/min | 13 | 14.5 |

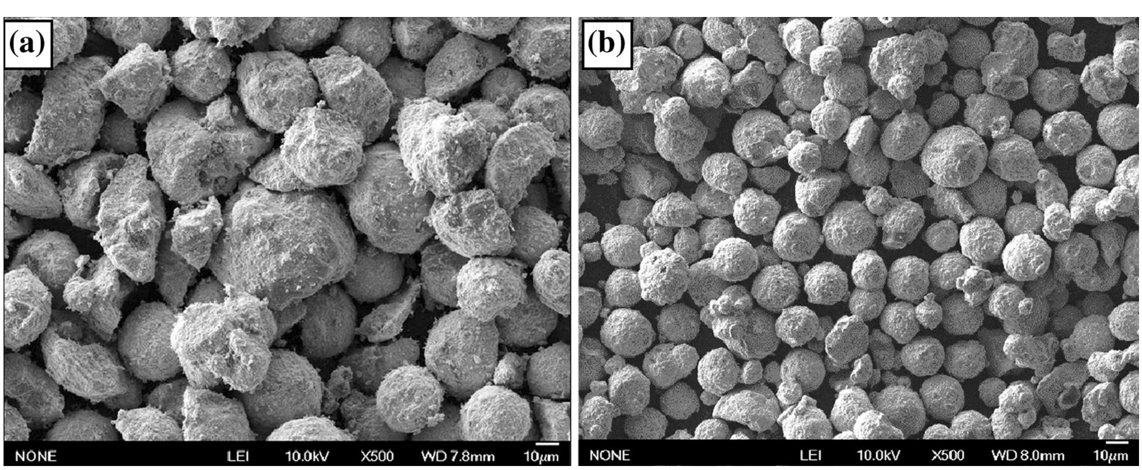


**Fig. 1** Micrographs of the WC-10Co-4Cr powders (a) Amdry 5843, (b) T62M150

### 2.4 Sand Slurry Erosion

Sand slurry erosion tests were performed in a homemade sand slurry erosion tester. The schematic diagram is shown in Fig. 2.

In these erosion wear tests, 40-70 mesh $SiO_2$ sand and fresh water were mixed in the hoper, and then accelerated by compressed air to impact the samples. The feed rate of sand was about 150 g/min and the mass ratio of sand to water was 1:10. The other testing parameters were 0.2 MPa air pressure, 25 mm erosion distance, 8 mm jet diameter, 30° and 90° impact angles. The sample was weighed every 15 min and six measurements were performed. For comparison, austenitic stainless steel AISI 316 samples were also tested under the same experimental conditions.

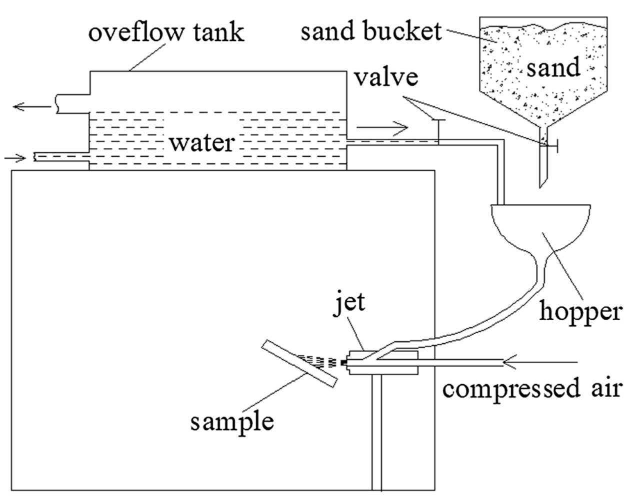


**Fig. 2** Schematic diagram of the sand slurry erosion tester

## 3. Results

### 3.1 Phase Composition of the Coatings

Figure 3 shows the XRD patterns of coatings prepared by the DJ2700 (HVOF) and the AK 07(HVAF) spray systems, as well as the corresponding WC-10Co-4Cr powders with different particle sizes (see Table 1)

The AK coating deposited by the HVAF spray process shows similar phase composition as the feedstock powder, mainly composed of WC with traces of $Co_3W_3C$ and crystalline Co, i.e., nearly no WC decarburization can be seen. The DJ coating deposited by the DJ2700-HVOF

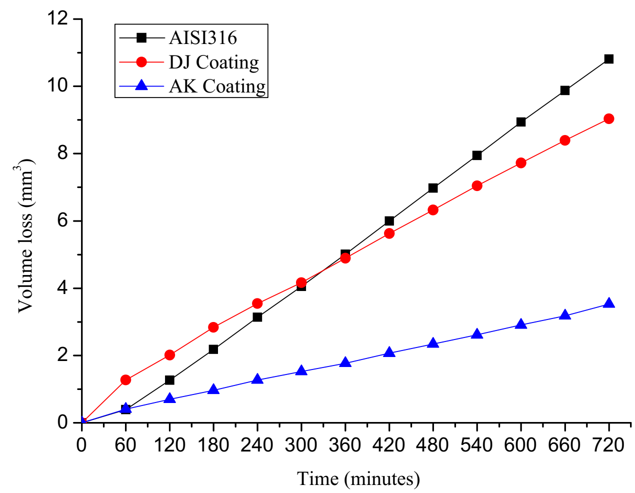


**Fig. 4** The cumulative cavitation volume loss of the AISI 316 stainless steel sample and the WC-10Co-4Cr coatings

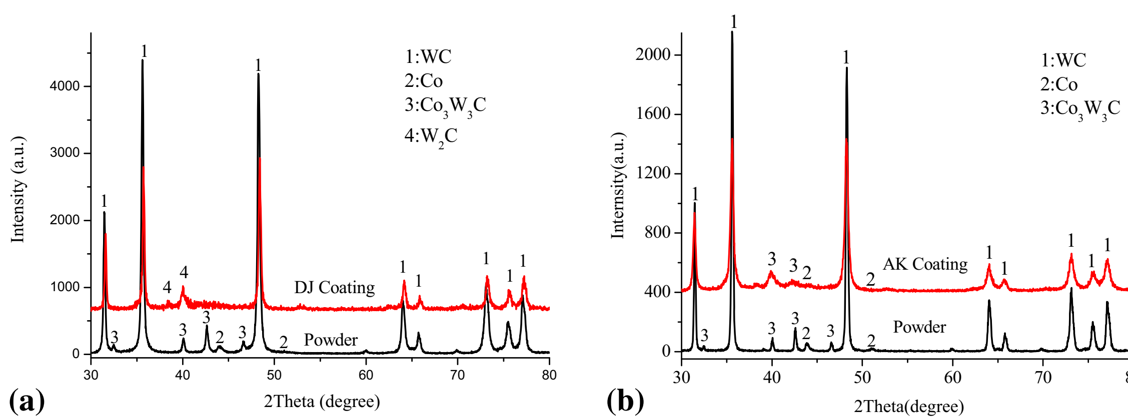


**Fig. 3** XRD patterns of the WC-10Co-4Cr powder and coatings (a) HVOF (b) HVAF

**Table 2 Properties of the HVOF- and HVAF-sprayed coatings and the AISI 316 stainless steel samples**

| Cavitation sample | Hardness, HV0.3 | Porosity, % | Fracture toughness, $MPam^{-1/2}$ | Surface roughness, Ra |
|---|---|---|---|---|
| AISI 316 stainless steel | $198.3 \pm 7.9$ | ... | ... | 0.38 |
| DJ coating | $1101.7 \pm 231.9$ | $0.90 \pm 0.14$ | $4.36 \pm 0.66$ | 4.67 |
| AK coating | $1229.4 \pm 200.8$ | $0.47 \pm 0.09$ | $5.86 \pm 0.57$ | 3.18 |

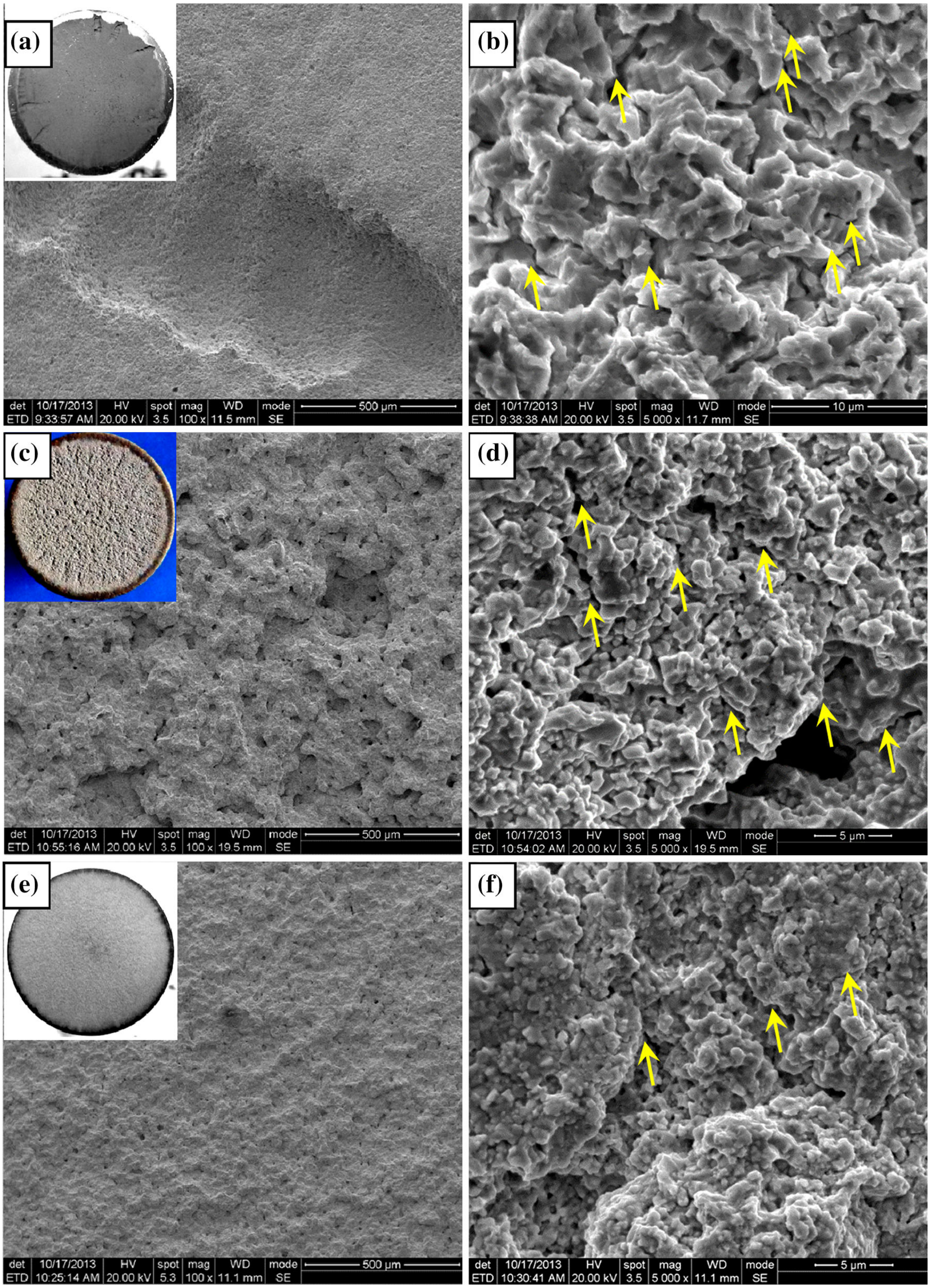


**Fig. 5** SEM images of the eroded surfaces of the AISI 316 stainless steel (a, b) and the WC-10Co-4Cr DJ (c, d) and AK (e, f) coatings after 720 min of cavitation test duration (the inset images are the surfaces of the cavitation samples, the yellow arrows point out cracks) (Color figure online)

system was composed of mainly WC and some $W_2C$ phases without $Co_3W_3C$, exhibiting some WC decarburization (Ref 5, 13). The $Co_3W_3C$ is a metastable phase, which is more likely to decompose in an HVOF flame at higher temperature, while stable in the HVAF flame at a lower temperature (Ref 14).

### 3.2 Mechanical Properties of the AISI 316 Stainless Steel Samples and the WC-10Co-4Cr Coatings

The data for hardness, porosity, fracture toughness, and the surface roughness of the two WC-10Co-4Cr coatings are presented in Table 2. For comparison, the hardness and the surface roughness of the AISI 316 stainless steel samples are also listed.

Table 2 shows that the AK coating exhibited higher average hardness, fracture toughness, but lower porosity and surface roughness than those of the DJ coating. The higher fracture

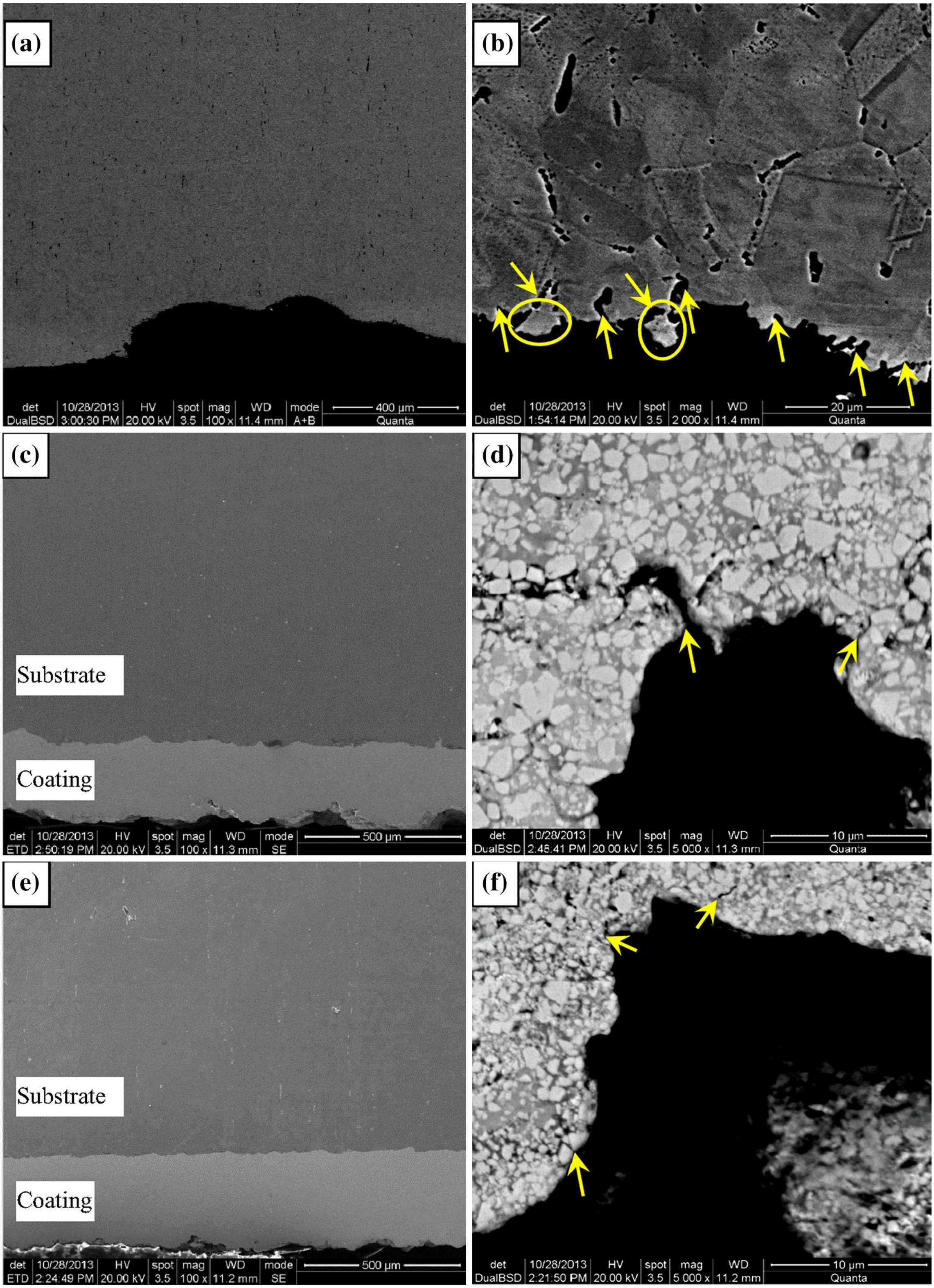


**Fig. 6** SEM images of the cross sections of the AISI 316 stainless steel (a, b) and the WC-10Co-4Cr DJ (c, d) and AK (e, f) coating samples after 720 min of cavitation test duration

toughness and low surface roughness for the AK coating can be, respectively, attributed to its lower degree of WC decarburization and finer particle size powder used.

### 3.3 Cavitation Resistances, Eroded Surfaces, and Cross Section of the Tested Samples

The cavitation results of the AISI 316 stainless steel sample and the two WC-10Co-4Cr coatings are presented in Fig. 4.

According to Fig. 4, the WC-10Co-4Cr coatings exhibited higher cavitation resistance than the AISI 316 stainless steel during the last 7 h of the test. Herewith, the AK coating revealed substantially higher cavitation resistance than that of the DJ coating in the whole test process. In addition, the DJ coatings exhibited higher cavitation erosion resistance than the AISI 316 stainless steel at the end of the test, although the DJ coating showed higher cumulative volume loss than the AISI 316 stainless steel at the beginning 60 and 300 min of the testing.

The macro- and micro-surface morphologies of the WC-10Co-4Cr coatings and the AISI 316 stainless steel sample after cavitation erosion testing are shown in Fig. 5. The AISI 316 stainless steel sample showed a relatively flat macro-eroded surface in the center and some lager radial pits on the perimeter region of the eroded surface (Fig. 5a). The AK coating sample also showed a relatively flat macro-eroded surface but without the large pits on its eroded surface (Fig. 5e). The DJ coating sample exhibited the roughest macro-eroded surface with many pits being visible (Fig. 5c).

The SEM images with different magnification of the cross sections of the AISI 316 stainless steel and the two WC-10Co-4Cr coating samples after cavitation testing are shown in Fig. 6. It can be seen that some pits and cracks occurred at the cross sections of all the tested samples.

Figure 7 shows the plot of the hardness variation with the distance from the surface of the AISI 316 stainless steel on its cross-section sample after cavitation erosion testing. An image of the tested sample is inserted in the figure, illustrating the regions where each hardness test was performed. It can be seen that the work hardening occurred at a thin surface layer (~0.3 mm) of the AISI 316 stainless steel sample.

### 3.4 Sand Slurry Erosion Resistance and Eroded Surfaces of the Tested Samples

The volume loss data for the AISI 316 stainless steel sample and WC-10Co-4Cr coatings from the sand slurry erosion tests are presented in Fig. 8.

From Fig. 8, it can be seen that the AISI 316 stainless steel showed much higher volume loss than those of the two WC-10Co-4Cr coatings in the sand slurry erosion testing. Comparing the two coatings, the DJ coating exhibited a little higher volume loss at both 30° and 90° impact angles than the AK coating. In addition, the DJ coating was worn out after 90 min of slurry erosion at a 90° erosion angle, so the cumulative volume loss data for this specimen were discarded.

SEM images of the sand slurry erosion surfaces of the AISI 316 stainless steel and the WC-10Co-4Cr coatings are shown in Fig. 9. It can be seen that the size of grooves and platelets on the eroded surfaces of the 316 stainless steel were larger than those on the surfaces of the DJ and AK WC-10Co-4Cr coatings at both 30° and 90° angles of impingement.

## 4. Discussion

### 4.1 Cavitation Behaviors of the AISI 316 Stainless Steel and the WC-10Co-4Cr Coatings

The higher cavitation erosion rate for the two coatings at the beginning of the testing can be attributed to their larger surface roughness and some relatively loose particles on the surfaces of the as-sprayed coatings.

The materials subjected to cavitation erosion can be destroyed by repeated short-time impacts (Ref 15). Some cracks induced by the cyclic micro-impact loads (marked by arrows in Fig. 5, 7b, d and f) were generated and propagated, and the material fatigued. A larger number of the particles (marked by the ellipses in Fig. 6b) were continuously pulled off from the tested samples according to their eroded surfaces and cross-section morphologies. It can be seen that the AISI 316 stainless steel and DJ coating have higher roughness and cumulative volume loss, while AK coating has lower cumu-

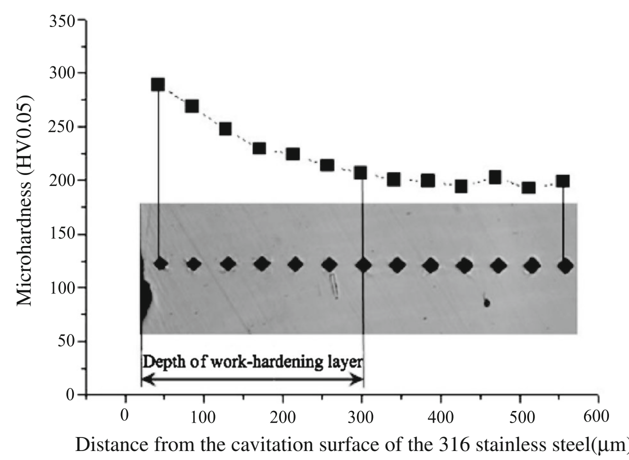


**Fig. 7** The hardness of the AISI 316 stainless steel on its cross section after cavitation erosion testing

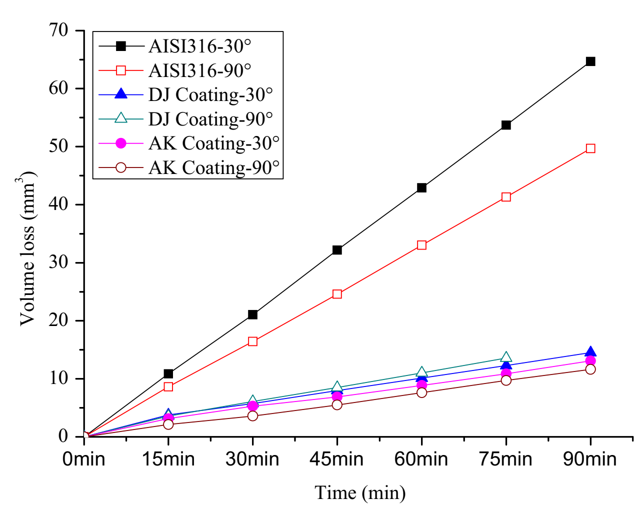


**Fig. 8** The cumulative and slurry erosion volume loss of the AISI 316 stainless steel sample and WC-10Co-4Cr coatings

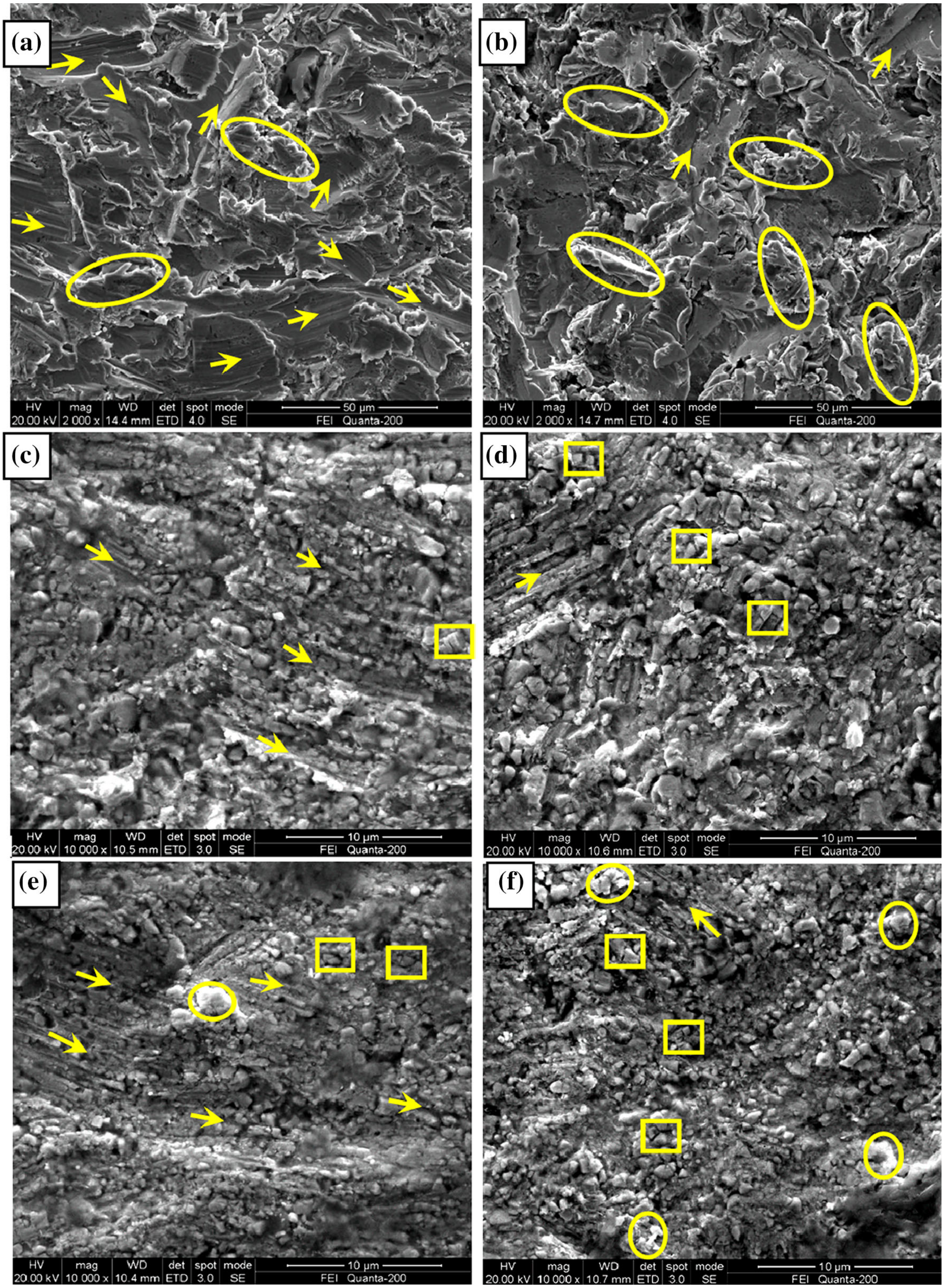


**Fig. 9** SEM images of the sand slurry erosion surfaces of the AISI 316 stainless steel and the WC-10Co-4Cr coatings: 30° (a) and 90° (b) for AISI 316 stainless steel; 30° (c) and 90° (d) for the DJ coating; 30° (e) and 90° (f) for AK coating

lative volume loss and the smoothest eroded surface after 720 min of cavitation testing according to Fig. 4, 5 and 6.

Wu et al. (Ref 16) proposed that the cavitation bubbles can easily nucleate at surface gouges and pores, and their presence can accelerate the damage caused by cavitation erosion. Their work shows that the existing damage pits or inherent porosity can initiate erosion damage. Since the AISI 316 stainless steel samples originally had the lowest surface roughness, this caused the relatively small degree of cavitation erosion at the beginning of the cavitation erosion testing. With the increase of the cavitation time, some small damage pits could occur. The cavitation bubbles were expected to nucleate and grow easily around these newly formed pits. Hence, the small damage pits, being continuously attacked during further cavitation, grew wider and deeper, which resulted in high cavitation erosion rate at the end of the test. From Table 2, it can be seen that compared to the DJ coating, the AK coating had lower surface roughness and porosity, which was responsible for its lower degree of cavitation erosion. In addition, the higher fracture toughness of the AK coating can also hinder the generation and propagation of the cracks during the cavitation erosion process, which may also explain its higher cavitation erosion resistance in comparison with the DJ coating.

Cavitation erosion is a steady-state damage process. The material surface subjected to the continuous impact, was continuously work hardened and then fractured. Hence, this thin work-hardened layer could have some contribution to the erosion resistance. The two coatings, however, exhibited no obvious hardening phenomenon.

### *4.2 Sand Slurry Erosion Behavior of the AISI 316 Stainless Steel and the WC-10Co-4Cr Coatings*

According to Fig. 4, the erosion behavior of the AISI 316 stainless steel exhibited typical erosion characteristics of ductile materials with the highest volume loss at both 30° and 90° impingement angles among all the tested materials. The DJ coating exhibited a little higher volume loss at 90° than at 30° erosion angle, which showed some characteristics of the brittle materials' erosion properties. The AK coating, however, showed some extent of the erosion properties of the ductile materials, which can be partially attributed to its high fracture toughness and the cobalt phase with a more obvious crystalline structure (Fig. 3).

After the 30° impingement tests, the eroded surfaces showed extensive plastic deformation and many grooves (marked by arrows in Fig. 9a, c, and e), and the main erosion mechanisms observed were micro-cutting and micro-plowing for the AISI 316 stainless steel and the WC-10Co-4Cr coatings. The lost and will be lost material platelets (marked by ellipses in Fig. 9a) were induced by the repeating impact of the erodent sand for the AISI 316 stainless steel. As for the two WC-10Co-4Cr coatings, it can be seen that the grooves might have formed predominantly in the softer binder region, leading to dislocation of the hard WC particles (Fig. 9c and e). The grooves in the binder region acted as failure initiating concentrators, and carbide grains were then cut off by the erodent sand (Ref 17). For the 90° impact angle, the dominating erosion mechanism of the AISI 316 stainless steel sample was the detachment of highly deformed platelets (Fig. 9b) as a consequence of the repeated impacts of the sand particles over the surface. For the two WC-10Co-4Cr coatings, the main erosion mechanism was that the soft Co-Cr binder was firstly cut and chiseled by the erodent sand particles, accompanied by the WC particles broken (marked by rectangles in Fig. 9c, d, e, and f). Finally, the WC particles were pulled off due to losing the support of the binder under the combined impact of the high-velocity erodent particles and water. A similar sand erosion mechanism has been reported earlier by Thakur and Arora (Ref 18).

In addition, the signs of micro-plowing and micro-cutting were still observed on the eroded surfaces of the AISI 316 stainless steel and the two WC-10Co-4Cr coatings after the 90° impingement tests. The reason was that the drag forces caused by the water presence could partially prevent the direct impact of particles against the surface (Ref 19). Compared with the two WC-10Co-4Cr coatings, the sizes of grooves and platelets on the eroded surface of the AISI 316 stainless steel are smaller (Fig. 9), which can be attributed by the following two reasons. (1) The erodent sand employed in the erosion experiment was $SiO_2$ whose hardness was higher than the AISI 316 stainless steel and the CoCr binder in the coatings, while was lower than the WC particles. The higher hardness of WC particles in the WC-10Co-4Cr coating can effectively hinder the micro-cutting, plowing, and chiseling of the erodent sand during the erosion process, which resulted in less erosion volume loss of the coatings than of the AISI 316 stainless steel. (2)Due to their high average macro-hardness coupled with medium toughness, the WC-10Co-4Cr coatings deposited by the HVOF process (DJ coating) and especially by the HVAF (AK coating) spray process can decrease the depth of grooves and the size of platelets caused by the erodent sand, and exhibit much higher erosion resistance than the AISI 316 stainless steel.

## 5. Conclusions

Two WC-10Co-4Cr coatings were deposited by the HVAF and HVOF spray processes, respectively. The phase compositions, mechanical properties, cavitation and sand slurry erosion resistances of these two as-sprayed coatings were investigated and compared to the AISI 316 stainless steel.

(1) The cumulative cavitation and sand slurry erosion volume losses of the two investigated coatings were lower than those of the AISI 316 stainless steel, which can be attributed to the higher average hardness of the coatings. In addition, the WC-10Co-4Cr coating deposited by the HVAF spraying process exhibited lower porosity, with higher hardness, fracture toughness, cavitation and sand slurry erosion resistances than the one produced by the HVOF spraying process.

(2) The cavitation erosion of the AISI 316 stainless steel and WC-10Co-4Cr coatings occurred due to the generation and propagation of cracks induced by the cyclic micro-impact loads, which led to a larger number of particles being continuously pulled off of the surface of the tested materials and the further materials fatigue.

(3) The micro-cutting and micro-plowing were the main mechanisms for the sand slurry erosion of both the AISI 316 stainless steel and the WC-10Co-4Cr coatings at the low impact angle, while the micro-cutting and micro-chiseling of the Co-Cr binder phase accompanied by the breaking and pulling off of the WC particles were the main mechanism for the sand slurry erosion of the WC-10Co-4Cr coatings at the high impact angle.

(4) The WC-10Co-4Cr coatings, especially those prepared by the HVAF spray process have a great potential for being used for the surface protection of hydro-turbine components against cavitation and sand slurry erosion.

### Acknowledgments

This research was supported by the Project of Training Targets of Young Key Teachers of Common College & University in

Hunan Province and the Project of Hunan Province Science and Technology Program (Grant No. 2013WK3027)

## References


1. R. Singh, S.K. Tiwari, and S.K. Mishra, Cavitation Erosion in Hydraulic Turbine Components and Mitigation by Coatings: Current Status and Future Needs, *J. Mater. Eng. Perform.*, 2012, **21**, p 1539–1551
2. F.T. Cheng, P. Shi, and H.C. Man, Correlation of Cavitation Erosion Resistance with Indentation-Derived Properties for a NiTi Alloy, *Scripta Mater.*, 2001, **45**, p 1083–1089
3. S.K. Singhal and S. Ratnendra, *Proceedings of the Himalayan Small Hydropower Summit*, Held During October 12-13, Dehradun, 2006, p 200-207
4. B.S. Mann and V. Arya, Abrasive and Erosive Wear Characteristics of Plasma Nitriding and HVOF Coatings: Their Application in Hydro Turbines, *Wear*, 2001, **249**, p 354–360
5. Q. Wang, J. Xiang, G.Y. Chen, Y.L. Cheng, X.Q. Zhao, and S.Y. Zhang, Propylene Flow, Microstructure and Performance of WC-12Co Coatings Using a Gas-Fuel HVOF Spray Process, *J. Mater. Process. Technol.*, 2013, **213**, p 1653–1660
6. L. Jacobs, M.M. Hyland, and M.D. Bonte, Study of the Influence of Microstructural Properties on the Sliding-Wear Behavior of HVOF and HVAF Sprayed WC-Cermet Coatings, *J. Therm. Spray Technol.*, 1999, **8**, p 125–132
7. A. Verstak and V. Baranovski, in: B.R. Marple, M.M. Hyland, Y.-C. Lan, R.S. Lima, J. Voger (Eds.), *AC-HVAF Sprayed Tungsten Carbide: Properties and Applications, Thermal Spray 2006: Building on 100 Years of Success*, ASM International, Seattle, A, May 15-18, 2006, (Paper 11827)
8. A. Verstak and V. Baranovski, *Deposition of Carbides by Activated Combustion HVAF Spraying, Thermal Spray Solutions: Advances in Technology and Application*, May 10-14, 2004 (Osaka, Japan), DVS, German Welding Society, 2004, p 551
9. S.L. Liu, X.P. Zheng, and G.Q. Geng, Influence of Nano-WC-12Co Powder Addition in WC-10Co-4Cr AC-HVAF Sprayed Coatings on Wear and Erosion Behavior, *Wear*, 2010, **269**, p 362–367
10. S. Matthews, M. Hyland, and B. James, Long-Term Carbide Development in High-Velocity Oxygen Fuel/High-Velocity Air Fuel $Cr_3C_2$-NiCr Coatings Heat Treated at 900 °C, *J. Therm. Spray Technol.*, 2004, **13**, p 526–536
11. Q. Wang, S.Y. Zhang, Y.L. Cheng, J. Xiang, X.Q. Zhao, and G.B. Yang, Wear and Corrosion Performance of WC-10Co-4Cr Coatings Deposited by Different HVOF and HVAF Spraying Processes, *Surf. Coat. Technol.*, 2013, **218**, p 127–136
12. I. Hulka, V.A. Şerban, I. Secoşan, P. Vuoristo, and K. Niemi, Wear Properties of CrC-37WC-18 M Coatings Deposited by HVOF and HVAF Spraying Processes, *Surf. Coat. Technol.*, 2012, **210**, p 15–20
13. A.G. Evans and T.R. Wilshaw, Quasi-Static Solid Particle Damage in Brittle Solids—I. Observations Analysis and Implications, *Acta Metall.*, 1976, **24**(10), p 939–956
14. O. Eso, Z.Z. Fang, and A. Griffo, Kinetics of Cobalt Gradient Formation During the Liquid Phase Sintering of Functionally Graded WC-Co, *Int. J. Refract. Met. Hard Mater.*, 2007, **25**, p 286–292
15. X.B. Zhang, C.S. Liu, X.D. Liu, J. Dong, and B. Yu, Cavitation Erosion Behavior of WC Coatings on CrNiMo Stainless Steel by Laser Alloying, *Int. J. Miner. Metall. Mater.*, 2009, **16**, p 203–207
16. S.K. Wu, H.C. Lin, and C.H. Yeh, A Comparison of the Cavitation Erosion Resistance of TiNi Alloys, SUS304 Stainless Steel and Ni-Based Self-Fluxing Alloy, *Wear*, 2000, **244**, p 85–93
17. I. Hussainova, J. Kübarsepp, and I. Shcheglov, Investigation of Impact of Solid Particles Against Hard Metal and Cermet Targets, *Tribol. Int.*, 1999, **32**, p 337–344
18. L. Thakur, N. Aroraa, R. Jayaganthan, and R. Soodc, An Investigation on Erosion Behavior of HVOF Sprayed WC-CoCr Coatings, *Appl. Surf. Sci.*, 2011, **258**, p 1225–1234
19. G.W. Stachowiak and A.W. Batchelor, *Engineering Tribology*, Butterworth-Heinemann, Oxford, 2005